Biosensors and Bioelectronics 124–125 (2019) 129–135

Contents lists available at ScienceDirect

Biosensors and Bioelectronics

journal homepage: www.elsevier.com/locate/bios

Non-invasive electromechanical cell-based biosensors for improved investigation of 3D cardiac models

Guido Caluori[a,b,c], Jan Pribyl[a], Martin Pesl[b,d,e], Sarka Jelinkova[d], Vladimir Rotrekl[d], Petr Skladal[a,*], Roberto Raiteri[c,*]

[a] Central European Institute of Technology, Masaryk University, Kamenice 5, 62500 Brno, Czech Republic
[b] International Clinical Research Centre of Saint Anne Hospital Brno, Pekarska 53, 60200 Brno, Czech Republic
[c] Department of Informatics, Bioengineering Robotics and Systems Engineering, University of Genova, Via All'Opera Pia, 13, 16145 Genova, Italy
[d] Department of Biology, Faculty of Medicine, Masaryk University, Kamenice 5, 62500 Brno, Czech Republic
[e] 1st Department of Cardiovascular Diseases, St. Anne's University Hospital and Masaryk University, Pekarska 53, Brno, Czech Republic

ARTICLE INFO

Keywords:
Excitation-contraction coupling
Human pluripotent stem cells
Cardiomyocytes
Atomic force microscopy
Microelectrode array
Drug testing

ABSTRACT

Cardiomyocytes (CM) placed on microelectrode array (MEA) were simultaneously probed with cantilever from atomic force microscope (AFM) system. This electric / nanomechanical combination in real time recorded beating force of the CMs cluster and the triggering electric events. Such "organ-on-a-chip" represents a tool for drug development and disease modeling. The human pluripotent stem cells included the WT embryonic line CCTL14 and the induced dystrophin deficient line reprogrammed from fibroblasts of a patient affected by Duchenne Muscular Dystrophy (DMD, complete loss of dystrophin expression). Both were differentiated to CMs and employed with the AFM/MEA platform for diseased CMs' drug response testing and DMD characterization. The dependence of cardiac parameters on extracellular Ca^{2+} was studied. The differential evaluation explained the observed effects despite variability of biological samples. The β-adrenergic stimulation (isoproterenol) and antagonist trials (verapamil) addressed ionotropic and chronotropic cell line-dependent features. For the first time, a distinctive beating-force relation for DMD CMs was measured on the 3D cardiac in vitro model.

1. Introduction

In the field of cell-based biosensors, cardiomyocytes (CM) are often used as models to study heart related diseases. The monitoring of electric activities of CMs is typically chosen; (multi)electrode transducers seem well established and widely available as microelectrode arrays (MEA) (Rothermel et al., 2005). The beating of CMs can be followed relatively easily (e.g. by video microscopy, Laurila et al., 2015), though in many situations the missing information on the associated beating force is of paramount importance in heart remodeling pathologies, such as dystrophinopathies and cardiomyopathies (Vatta et al., 2005). Beating force is associated with pathophysiological electro-mechanical coupling, and its alterations result often in mechanical heart failure (Pesl et al., 2016a). Such biomechanical measurements investigating the dilated cardiomyopathy were previously done on CMs using the stretcher device (Knoll et al., 2002). More detailed investigations were later done using cantilevers as nanomechanical transducers and atomic force microscope (AFM) as the evaluation system in real time with individual cardiomyocyte cells (Liu et al., 2012a,2012b) or cell clusters (Pesl et al., 2016a). Thus, combination of AFM for biomechanical changes with MEA sensing electric signals described here seems naturally promising for elucidating complex events in cardiomyocytes obtained from patient derived stem cells. This approach provides a robust and convenient example of the organ-on-a-chip system demonstrating its capabilities on disease related CMs.

Supplementary material related to this article can be found online at doi:10.1016/j.bios.2018.10.021.

The introduction of human pluripotent stem cells (hPSC, either embryonic, hESC, or induced pluripotent, hiPSC) and cardiac differentiation protocols allowed almost two decades of study on the cardiac organogenesis and functionality. In particular, patient-specific hiPSC representing a direct supply of healthy and mutation-carrying samples (Sinnecker et al., 2014) allow for description of the diseases progression involved in heart failure (Moretti et al., 2013). To improve the comparison between in vitro models, CRISPR-Cas9 technology has recently gained an outstanding popularity for its efficiency and flexibility in inducing precise mutations in cell lines, providing researchers with isogenic controls (Motta et al., 2017). hPSC-derived cardiomyocytes

* Corresponding authors.
E-mail addresses: skladal@chemi.muni.cz (P. Skladal), roberto.raiteri@unige.it (R. Raiteri).

https://doi.org/10.1016/j.bios.2018.10.021
Received 1 July 2018; Received in revised form 11 October 2018; Accepted 11 October 2018
Available online 16 October 2018
0956-5663/

and models recapitulate the morphological, genetic and functional characteristics of the heart muscle, specifically the subcellular cascade known as cardiac excitation-contraction coupling (cECC), responsible for heart pumping function (Bers, 2002). Cardiomyocytes from hPSC can be derived as 2D or 3D stem cell cultures. However, the 3D models seem to be superior and more physiologically relevant compared to the 2D ones (Regmi and Jeong, 2016). For monolayer culture, the multiple existing protocols with high differentiation efficiency involve modulation of the canonical Wnt/β-catenin pathway (Lian et al., 2012; Burridge et al., 2014), with high differentiation efficiency. For 3D cultures, the protocols exploit the spontaneous differentiation triggered from the aggregation of hPSC into embryoid bodies, which is driven to cardiac phenotypes using hypoxia and small molecules cocktails (Pesl et al., 2014). The efficiency of differentiation and grade of maturation can vary according to protocol and cell lines, and can be improved by physical methods, as in electro-mechanical stimulation (Bauwens et al., 2016). Purified hPSC-CMs can be further reassembled in precise geometries, such as in the engineered heart tissue (Tzatzalos et al., 2016). From gene expression to functionality, hPSC-CMs present an embryonic-like cardiac phenotype, with immature sarcomeres, sarcoplasmic reticulum and calcium cycling (Mummery et al., 2012; Acimovic et al., 2014). An immature phenotype has also been proven for embryoid body-derived cardiac models (Doevendans et al., 2000). Nevertheless, hPSC-CMs play a key role in future drug development with reduced attrition rate (Liang et al., 2013; Zheng et al., 2013), in cardiotoxicity assays (Takeda et al., 2018), disease modeling (Dell'Era et al., 2015) and in cell-based regenerative therapies (Doppler et al., 2013), and further studies to achieve cardiac maturation are ongoing. This aspect is also investigated by our proposed approach, to assess its robustness.

The hPSC-derived cardiac models can be characterized by functional (or phenotypic) properties though multiple in vitro assays, reviewed in another work from our group (Pesl et al., 2016b). Among these, atomic force microscopy has in the past three decades achieved remarkable role in the evaluation of biological samples mechanics and topography (Alonso and Goldmann, 2003; Kilpatrick et al., 2015) in native culture environment. In particular, it has been employed in important studies on single CMs (Liu et al., 2012a). A combination of AFM and 3D cardiac models has already been proposed as cell-based biosensor (CBB) in our previous work (Pesl et al., 2016a). Most AFM systems are now currently integrated with optical and confocal microscopy, which allows the implementation of combined measures of AFM and calcium imaging (Liu et al., 2012b; Caluori et al., 2018), but further systems can be included if properly miniaturized. Small biosensors, such as microelectrode arrays (MEA), can be engineered to comply with AFM and optical microscopy systems for cardiac investigation (Cogollo et al., 2011). The attractiveness of MEA-based electrophysiology resides in its ability to multiprobe extracellular field potentials (EFP) of electroactive cells in a non-destructive fashion, which allows for prolonged and complex measurements of cells and tissues (Spira and Hai, 2013).

In this work, we present an electromechanical in vitro system for the combined study of cECC on 3D cardiac models, employing both AFM and MEA platforms together. The aim of this work is to provide an improved method for cardiac models characterization and drug testing in the format of an organ (heart)-on-a-chip. For this reason, we have confronted a model of cardiac maturation with respect to its control, and employed a disease model of Duchenne muscular dystrophy (DMD), a progressively invalidating pathology of the striated muscle, including the myocardium (Finsterer and Stöllberger, 2003).

2. Materials and methods

2.1. hPSC culture and cardiac differentiation

The cardiac cells clusters were obtained using the hESC line CCTL14 (Adewumi et al., 2007) and one hiPSC line reprogrammed from fibroblasts of a patient affected by Duchenne Muscular Dystrophy (DMD). The patient carries a deletion of exons 45–50 of the DMD gene causing a complete loss of dystrophin expression. The line has been fully characterized for pluripotency markers (https://hpscreg.eu/cell-line/MUNIi001-A) and the differentiated CMs were tested for presence of striated pattern of sarcomeres labeled with cardiac troponin T (sc-8121, Santa Cruz), and cytoplasmic presence of dystrophin (NCL-DYSB, Leica) (see Supplementary material, SFig. 1). Pluripotent cells were firstly thawed and seeded on mitotically-inactivated mouse embryonic fibroblasts (feeder cells). The hPSC colonies were cultivated in DMEM-F12 (Thermofisher, Waltham, MA, USA) supplemented with 15% KnockOut fetal bovine serum Serum Replacement (FBS, Life Technologies, Carlsbad, CA, USA), 1% L-glutamine (Thermofisher), 0.5% penicillin/streptomycin (Thermofisher), 1% 2-mercaptoethanol (Thermofisher), 1% non-essential amino acids (Life Technologies), and 4 ng ml^{-1} and 10 ng ml^{-1} human fibroblast growth factor 2 (hFGF2, Peptrotech, London, UK) for hESC and hiPSC, respectively. Medium was changed daily and colonies were propagated for at least 5 passages, by manual fractioning. hESC cells were divided in a control group (CTRL) and another group (DORSO) undergoing an exposure to 500 nM of dorsomorphin (Sigma Aldrich, St. Louis, MO, USA) 4 days to the differentiation protocol, to improve cardiac commitment (Hao et al., 2008).

Cardiac differentiation was started by embryoid body formation, as described elsewhere (Pesl et al., 2013). Briefly, compact, round colonies were manually cut and scratched from the culture surface. For DMD iPSC, the colonies were kept intact, carefully detached from the culturing surface as a whole. The cell leaflets were transferred in hypoxic incubation atmosphere (5% O_2) and underwent a sequential cytokine modulation in KnockOut DMEM (Life Technologies), supplemented with 10% FBS, 1% L-glutamine, 1% PS, 1% 2-mercapthoethanol, 1% non-essential amino acids (further referred simply as culture medium). Beating cardiac clusters (BCC, Supplementary Fig. 1) were visible from day 14 and were transferred into normoxic atmosphere. After day 22, they were kept in the culture medium with 10 μg ml^{-1} ascorbic acid (Sigma Aldrich).

2.2. Microelectrode arrays cleaning and coating

Before beating CMs cluster plating, 60 channel MEAs (60MEA200/30iR-Ti/ITO, Multichannel Systems, Reutlingen, Germany) were cleaned using a 0.1% w/v solution of Tergazyme detergent (Alconox, White Plains, NY, US) in MilliQ water for at least 8 h. The culture well (i.e. the area inside the plastic ring) was then thoroughly washed with MilliQ water to remove the excess detergent. The preparation of the device was moved to a UV-sterilized clean box (Biosan, Riga, Latvia). Each MEA was placed in 100 mm sterile Petri dish (TPP, Trasadingen, Switzerland), and the MEA culture well was sterilized by filling it with 70% ethanol solution. After 30 min, the sterilizing solution was removed, the culture well on MEA was rinsed twice with 0.2 μm-filtered MilliQ water and let dry. The sensing area (i.e. the electrode array area) was then coated with 20–50 μl of 0.1 mg ml^{-1} laminin (Sigma Aldrich) and fibronectin (Sigma Aldrich) mixture, 1:1 ratio, to promote cell adhesion. The MEAs were put in a cell incubator at 37 °C, 5% CO_2, overnight. The next day, MEAs were rinsed twice with filtered MilliQ water to remove excess of adhesion factor from the surface.

2.3. BCCs plating on MEA chips

Suspended BCCs were collected and plated on MEA sensing area with 30 μl droplet of the culture medium. This amount of medium was a safe tradeoff between sample wobbling limitation and the need of hydrated environment. Samples were manually placed on top of electrode array, then put in standard cell incubator and kept in this overnight (with loosely fitted lid and additional droplets were placed separately around the well to prevent evaporation). The following day, medium

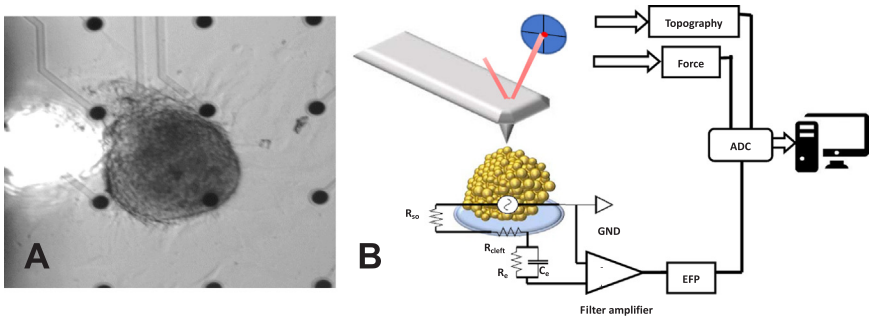

Fig. 1. Real case and schematic of the proposed electromechanical cell-based system. A) A beating cardiac cluster (BCC) placed on a microelectrode array (MEA) sensing area. The bright spot on the left side represents the AFM laser reflecting from the cantilever. Scale bar is 200 μm. B) Schematic representation of the implemented setup. The BCC acts as a periodic micro-voltage generator sensed by the planar electrode, while the AFM measures the topographical displacement and the exerted force. The synchronous acquisition is guaranteed by the common acquisition board and computer.

was gently added atop up to 1 ml. The BCCs were allowed to stabilize up to 3 days in vitro to ensure appropriate adhesion, spreading and formation of cell-electrode contacts. Fig. 1A and Supplementary Fig. 3 show typical BCCs properly placed on MEA, before beginning the experiments. Supplementary video recording presents movements of the adhered BCC clearly demonstrating the regular beating events.

2.4. Setup preparation and experimental protocols

The MEA chip containing the samples was housed in a customized holder made of an aluminum plate with adhesive heating pads and Pt100 temperature probe (RS Components, Corby, UK), and an electronic board with contacts to interface with the MEA electrodes. The electronic board was equipped with 60-channels unity-gain amplifiers to provide low impedance tracks and noise shielding. A second filtering-amplifying stage provides a pass-band of 10–3000 Hz and a total gain of 60 dB. The described holder was then fixed on the motorized stage of an inverted microscope (Olympus IX-81S1F-3, Tokyo, Japan). An AFM scanner head with 15 μm vertical range (BioAFM NanoWizard 3, JPK, Berlin, Germany) was placed above the sample. A soft silicon nitride cantilever SNL-10-D (Bruker, Billerica, MA, USA; nominal spring constant 30 pN m^{-1}) was used as nanomechanical probe to ensure stable contact without applying disruptive forces on the sample. The cantilever spring constant was calibrated before each experiment using the thermal noise method (Butt and Jaschke, 1995). A contact force of 5 nN was found optimal compromise between baseline stability and absence of visible adverse effects on the sample, as previously showed (Pesl et al., 2016a). Each experiment was performed in Tyrode solution (135 mM NaCl, 10 mM HEPES, 5.4 mM KCl, 0.9 mM $MgCl_2$, pH 7.4) supplemented with 10 mM glucose and 1.8 mM $CaCl_2$. After solution exchange, the calibrated cantilever was immersed in liquid and put in contact with the sample several times to identify the superficial center of contraction (i.e. the point with highest vertical positive displacement). Once the center of contraction was found, the drug trials started at an interval of 5 min of recording and 10 min settling time after drug administration or washout (a schematic is provided in Supplementary Fig. 4).

Calcium chloride solution was obtained in Tyrode buffer to give a stepwise increment of 1.1 mM after each addition. Isoproterenol stock solution (30 μM) was made in sterilized MilliQ water to prevent it from quenching: the selected step increment was 300 nM. Finally, Verapamil hydrochloride (Lekoptin, Lek Pharmaceuticals, Ljubljana, Slovinia) stock solutions (127.5 μM) were made in Tyrode, for a step increment of 255 nM. The added volume of drug solution never exceeded 5% of the basal volume in the MEA chip (2 ml).

2.5. Data recording and evaluation

All the presented protocols were repeated on 3 biological replicates of each cell line. Electromechanical recordings were acquired at 5 kHz sampling frequency through a LabVIEW virtual instrument and a proprietary data acquisition board PCI6071E (National Instruments, Austin, TX, USA). Fig. 1B shows a schematic of the acquisition system. Cell mechanocardiogram (MCG) comprehends the time-dependent topographical changes (i.e. the vertical displacement of the AFM piezo actuator, in μm) and the uncompensated force (in nN). The cell-cantilever contact was never lost during drug injections or medium washout. The obtained data were post-processed and analyzed using a Matlab R2016b (Natwick, MA, USA) GUI, using state of the art algorithms. From each recording, the parameters listed in Table 1 and defined in Supplementary Fig. 5 were determined. Statistical analysis was performed in Prism 5.0 (GraphPad Software, La Jolla, CA, USA) and numerical results are presented as mean ± SEM, after passing normality test. Datasets were compared for statistical significance using 1-way analysis of variance (ANOVA) with Bonferroni post-test, or repeated measures 2-way ANOVA with matching on drug concentration levels. Statistical significance was accepted with p-values below 0.05.

3. Results and discussion

3.1. Simultaneous electromechanical recording

The implemented setup allowed the simultaneous visualization, synchronous recording and coupled analysis of the electromechanical features of the cECC (Fig. 2A). The lowest observable noise level in the MEA-EP traces was 33.3 μVpp, whereas the average noise in the force and in the Z height traces were 18.3 pN and 24.5 nm respectively. Online and post-processing digital filtration allowed the analysis of

Table 1
Description of extracted parameters.

Parameter name	Description
Beating rate	Reciprocal of time distance between two adjacent events
Electro mechanical delay	Time between the electrical event and 10% of the next contraction maximum amplitude
Contraction time	Time between 10% of the peak amplitude and the peak, on the rising side
Relaxation time	Time between the event peak and the point corresponding to 10% of the peak amplitude on the falling side
Duration time	The sum of contraction and relaxation times
Average speed of contraction	Mean of the first derivative of the rising part of contraction
Time constant	Time parameter obtained by fitting the relaxation time interval with a decreasing exponential function
Force	The uncompensated force peak-to-peak during the contraction
Z height	The peak excursus of the AFM Z-piezo following the contraction

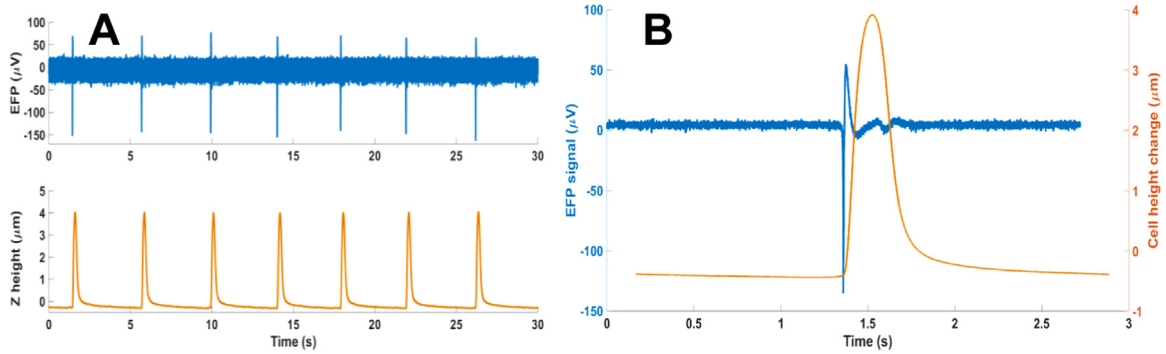

Fig. 2. Representative recording obtained with the implemented electromechanical system, and its post-processed part. A) Simultaneously and synchronously acquired extracellular field potential (top) and mechanical contraction (bottom). B) Averaged curves from the same recording; it is possible to appreciate the noise reduction due to filtering. The two traces are separated by the mean calculated delay.

EFPs with signal-to-noise ratio even close to 0 dB. Nevertheless, approximately half of the plated samples were able to produce a visible EFP trace, while mechanically beating. This issue is most probably due to scarcely-conductive coupling between the MEA planar electrodes and the BCC. Extracellular biopotentials morphology is fundamentally dependent on the conductive sample/electrode proximity and high resistance cleft (Spira and Hai, 2013). As BCC present a mixed cell population of cardiomyocytes and fibroblast-like cells (Supplementary Fig. 1A), as also previously reported (Ma et al., 2011); it is plausible that a non-conductive patch might adhere to the electrode area. In fact, fibroblast-like cells are found to be dedicated into BCC adhesion and spreading (Supplementary Fig. 2). This drawback is easily amendable, since it is possible to remove gently and re-plate BCCs in sterile conditions.

Each measurement lasted between 4 and 5 h, without any remarkable alteration of cardiac activity, if not due to drug stimulation. This can be also seen in the absence of morphological alteration between beginning and end of protocol (Supplementary Fig. 3). Although probed in not completely sterile conditions, it was found that if refilled with antibiotics-containing medium, at the end of the experiments, the samples can keep on without visible contamination up to 4 days. This is particularly useful when testing overnight or realizing several-day treatments. Such evidence shows, like previously reported, how the adopted BCC model presents an outstanding resilience. Since an applied force of 5 nN did not elicit any spontaneous change in the measured parameters, in time, one can infer that the implemented CBBs are really following alteration of cECC and not mechano-electric feedback from stretch-induced depolarization (Zhang et al., 2008).

An accurate peak detection and averaging period selection allowed the reconstruction of important physiological parameters described in Table 1, namely beating rate, contraction speed, cardiac cycle duration and, most importantly, a coupled parameter such as the electro-mechanical delay (EMD). To our best knowledge, this is the first time that such parameter is measured on 3D cardiac in vitro model. Fig. 2B shows the obtainable averaged electromechanical events, corrected by the calculated EMD.

3.2. Differential drug response and correlation analysis is indispensable to distinguish cell-type dependency of cardiac parameters

Once the feasibility and features of the implemented electromechanical CBBs were assessed, we firstly asked whether basal conditions would be sufficient to distinguish diseased and healthy hPSC derived BCC. The baseline beating frequency for all the cell lines tested was not significantly different (0.327 ± 0.023 Hz for CTRL, 0.325 ± 0.062 Hz for DORSO and 0.468 ± 0.103 Hz for DMD). The same evidence was found for other important functional parameters, such as the basal force (2.1 ± 1.9 nN for CTRL, 12.0 ± 4.7 nN for DORSO and 0.89 ± 0.46 nN for DMD) and EMD (23.0 ± 1.3 ms for CTRL, 22.0 ± 3.0 ms for DORSO and 25.6 ± 5.3 ms for DMD). Therefore, different stimulation / inhibition drug protocols were tested to validate the adopted models versus the expected cardiac response and assess the presence of cell type-dependent differences.

3.3. Calcium trials

Initially, the dependence of cardiac parameters on extracellular Ca^{2+} concentration was tested. This ion and its extracellular availability are in fact of primary importance for cECC, particularly for the hPSC-derived CMs, which possess an immature calcium handling toolkit (Keung et al., 2014) and rely mostly on membrane transport (Youm, 2016). Cell type-dependency was found by 2-way ANOVA for beating rate ($p = 0.007$), contraction duration ($p = 0.0003$), time decay ($p < 0.0001$) and EMD ($p = 0.026$). A difference close to significance was reached for the average speed of contraction ($p = 0.069$). The effect of the Ca^{2+} concentration was found significant only in relationship to the beating rate ($p < 0.0001$). All cell lines experienced a decrease in beating rate proportional to Ca^{2+} concentration. The CTRL and DORSO groups plateaued around ¾ of the basal rate (67 ± 10% and 68.6 ± 5.1%, respectively), while the DMD group decreased to 89.5 ± 3.2% of its basal rate. The beating rate phenotype of mutation-carrying cell line correlates with previously described pre-existing calcium stress impairing inward ion flux (Fanchaouy et al., 2009). This frequency decrease was paralleled by an increase of exerted force in all the cell lines (120.3 ± 9.4% for the CTRL group, 110 ± 14% for DORSO and 112 ± 19% for DMD). This phenomenon is due to the immature contractile phenotype of hPSC-derived CMs, which possess negative frequency-force relationship (Pesl et al., 2016b). The observed change of contractile events was found as an increase of the relaxation period, expressed by the decay time constant for the CTRL and DORSO groups (108.1 ± 3.5% and 110.5 ± 4.2%, respectively) and a decrease for DMD (84.3 ± 5.2%). The Ca^{2+} dependent decay time decrease in dystrophin mutation-carrying line is in correlation with previously described pre-existing calcium overload (Fanchaouy et al., 2009), which may limit the contraction dilation due to saturated sarcomere, probably resulting in limited ability of the DMD CBB to employ force imposed reaction during cluster stretch as imposed in healthy tissue by Frank Starling mechanisms. The EMD, a parameter directly connected to electromechanical coupling, did prove statistically significant for cell-type. CTRL did not show a dose-dependent relation with the Ca^{2+} concentration (109–99% variation range); DORSO showed a similar trend with only non-significant increase with respect to CTRL (142–131%), validating the CBB's robustness toward line specific variability in differentiation efficiency. Conversely, the DMD group showed a dose-dependent trend (up to 257 ± 71% of the basal delay); it is possible that increasing calcium levels are gradually

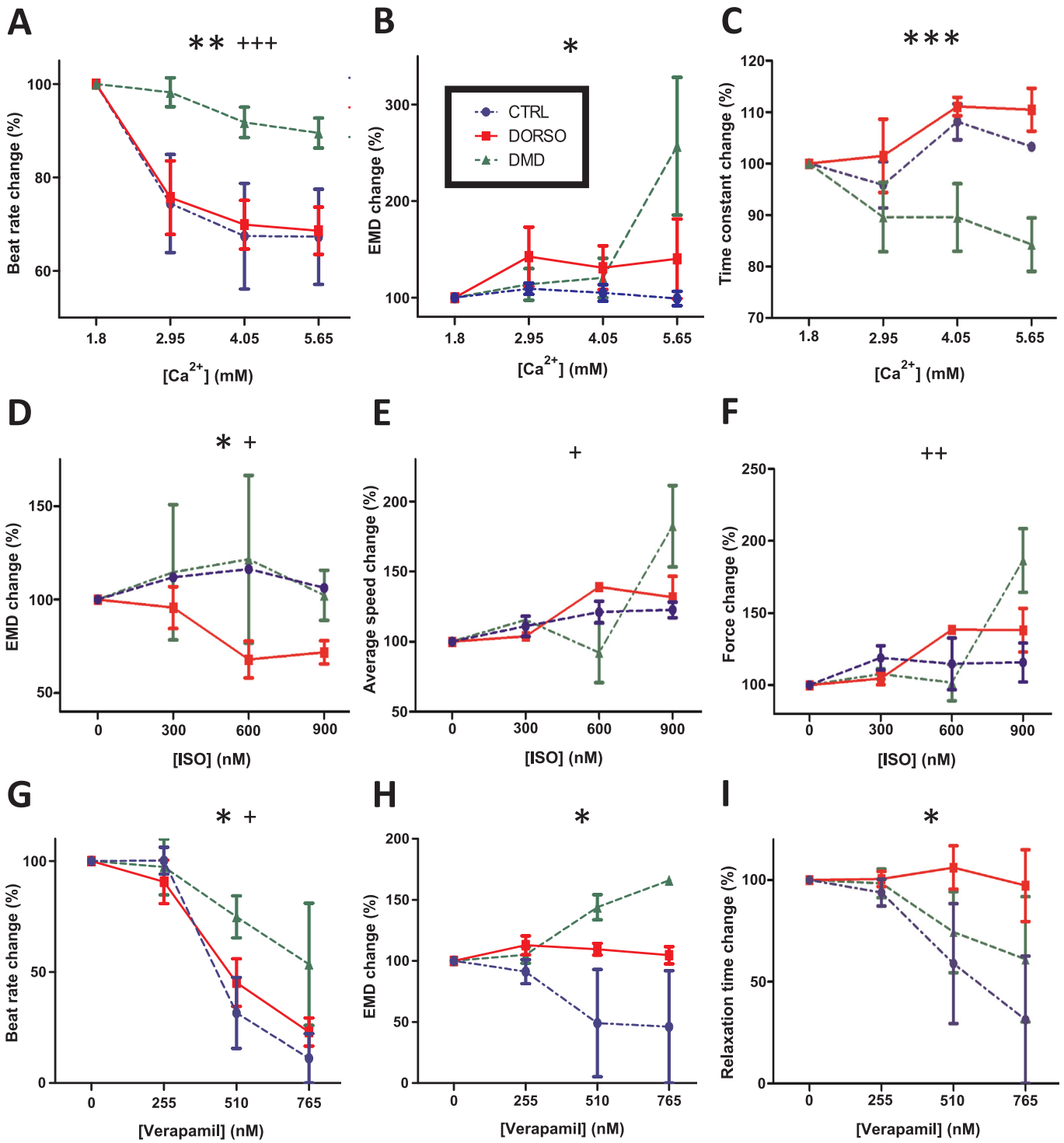

Fig. 3. Selected results of drug trials performed with the presented electrochemical cell-based biosensor. The top row (A-B-C) represents extracellular calcium concentration trials. The middle row (D-E-F) β-adrenergic stimulation trials (Isoproterenol). The bottom row (G-H-I) represent class IV antiarrhythmic / calcium channel blocker trial (Verapamil). The * symbol indicates statistically significant difference according to the beating cardiac cluster type. The + symbol indicates statistically significant difference due to the chemical concentration. One symbol indicates a p-value < 0.05, two symbols < 0.01, three symbols < 0.001. All the comparisons are carried on with repeated measurements 2-way ANOVA with row matching (drug concentration).

impairing the already elevated activity of an altered ryanodine receptor to coordinate the calcium-induced calcium release (Fauconier et al., 2010). The previous results are summarized in Fig. 3A-C.

3.4. Isoproterenol trials

The β-adrenergic stimulation was performed via increasing isoproterenol concentration to assess the ionotropic and chronotropic cell line-dependent features. Surprisingly, no extracted parameter showed significant dependency over the cell type, except for the EMD ($p = 0.0130$), which was also significantly concentration dependent ($p = 0.012$). Other concentration-dependent parameters were the average speed of contraction ($p = 0.031$) and the exerted force ($p = 0.006$), with DMD group showing marked increase at end

concentration (182 ± 29% and 186 ± 22% respectively). In contrast, DORSO experienced roughly 1/3 increase of these parameters (132 ± 15% for average speed and 138 ± 15% for force) and CTRL only 1/5 increase (122.7 ± 5.5% and 116 ± 14% respectively). Isoproterenol effect appears to have a threshold concentration between 300 and 600 nM. After this threshold, the CTRL and DMD groups slightly altered EMD (101.0 ± 6.0% and 96.6 ± 2.7%, respectively), whereas the DORSO group decreased its measured EMD to 73.0 ± 7.6% of the baseline value. This difference might be explained with better differentiation grade of dorsomorphin-treated groups, since dorsomorphin is an inhibitor of BMP signaling and promotes cardiac differentiation (Kattman et al., 2011). It is therefore plausible that an improved differentiation guarantees a better BCC syncytium, able to improve cECC timing in response to adrenergic stimulation. The notable results are shown in Fig. 3D-F. The same negative beating rate/force relationship was also noticed for all the cell lines, except when an arrhythmic behavior (e.g. multiple beating modes) was induced.

3.5. Verapamil trials

The antagonist trials were carried on L-type calcium channels to observe the reaction of different BCCs to class IV antiarrhythmics. Verapamil, as an example of this class, was shown to improve skeletal muscle force in DMD patients but led also to adverse cardiac side effect. However, no data on mechanism of such adverse effect exists (Nascimento Osorio et al., 2018). Previously, the growing CMs were coupled to RTCA impedance system, which allowed to quantify only beat rate effects of Verapamil (Wang et al., 2013). Here, the beat rate influence of drug showed to be cell type-dependent ($p = 0.019$) and dose dependent ($p = 0.001$). The EMD parameter was found to be only cell-type dependent ($p = 0.0316$), together with the relaxation time ($p = 0.030$). The measured exerted force and Z height change were found solely dose-dependent ($p = 0.015$ and $p = 0.019$ respectively). The DMD cells showed decrease in beating rate down to 53 ± 27% of baseline, compared to 11 ± 11% of CTRL and 23.0 ± 6.3% of DORSO groups. The EMD shows different trends for each cell line: for the CTRL groups, the delay drops to 46 ± 46% of the baseline; DORSO group upped to 112% of the baseline and ended the trial at 104.0 ± 7.1%; the DMD group showed an increase of 143% to finish the trial at 111 ± 55%. These distinct trends can be due to the different biological backgrounds of the BCC models: CTRL group may respond to L-type channel inhibition by referring to the inositol-3-phosphate complex, which spontaneously produces calcium influx in embryonic cardiac phenotype (Youm, 2016); dorsomorphin-treated BCC might express higher number of functional L-type calcium channels, therefore being more resilient to the same drug concentration and present delayed coupling, with stable force level. DMD samples can present calcium leaking at the membrane level (Burr and Molkentin, 2015), although cECC delay is linearly increasing, which together with the decreasing force suggests impairment of the contractile machinery (Li et al., 2014). The mentioned notable results are shown in Fig. 3G-I.

4. Conclusions

We have successfully implemented and tested the electro-mechanical cell-based biosensor for the simultaneous and synchronous probing of cardiac excitation-contraction coupling. The system allows the characterization of cardiac models through differential drug trials and sample-type discrimination. For the first time, to our knowledge, a distinctive beating-force relation was shown for Duchenne muscular dystrophy cardiac models. The bioelectromechanical parameters derived from the cardiomyocyte cluster based models provide important insights into heart pathologies and sometimes (such as in β-adrenergic stimulation assays) serve as the only discriminant between different models.

Current limitations of the systems regard the non-sterility of the measurement environment, and the localized probing of a 3D model with a single MEA electrode and AFM cantilever. The system also suffers from a substantial biological sample variability, which requires more experimental repetitions to achieve better accuracy of results; this can be overcome by suitable choice of drug treatment regimens to focus the data collection toward the desired disease phenotype. Future improvement with higher-density electrode arrays and tip-less cantilevers providing a wider surface contact should provide a higher information content and improve stability of models, respectively.

Acknowledgments

This research has been financially supported by the Ministry of Education, Youth and Sports of the Czech Republic under the project CEITEC 2020 (LQ1601) and ICRC (LQ1605), the CIISB research infrastructure project LM2015043 supported the AFM measurements at the Core Facility Nanobiotechnology, and the Grant Agency of the Czech Republic (GACR) provided support through grant no. P302/12/G157.

Conflict of interest

The authors declare no conflict of interest.

Appendix A. Supporting information

Supplementary data associated with this article can be found in the online version at doi:10.1016/j.bios.2018.10.021.

References

Acimovic, I., Vilotic, A., Pesl, M., Lacampagne, A., Dvorak, P., Rotrekl, V., Meli, A.C., 2014. Biomed. Res. Int. 2014, 512831.
Adewumi, O., Aflatoonian, B., Ahrlund-Richter, L., Amit, M., Andrews, P.W., Beighton, G., Bello, P.A., Benvenisty, N., Berry, L.S., et al., 2007. International stem cell initiative. Nat. Biotechnol. 25, 803–816.
Alonso, L., Goldmann, W.H., 2003. Life Sci. 72, 2553–2560.
Bauwens, C.L., Toms, D., Ungrin, M., 2016. J. Vis. Exp. 115, e54308.
Bers, D.M., 2002. Cardiac excitation–contraction coupling. Nature 415, 198–205.
Burr, A.R., Molkentin, J.D., 2015. Cell Death Differ. 22, 1402–1412.
Burridge, P.W., Matsa, E., Shukla, P., Lin, Z.C., Churko, J.M., Ebert, A.D., Lan, F., Diecke, S., Huber, B., Mordwinkin, N.M., Plews, J.R., Abilez, O.J., Cui, B., Gold, J.D., Wu, J.C., 2014. Nat. Methods 11, 855–860.
Butt, H.-J., Jaschke, M., 1995. Nanotechnology 6, 1–7.
Caluori, G., Pribyl, J., Cmiel, V., Pesl, M., Potocnak, T., Provaznik, I., Skladal, P., Rotrekl, V., 2018. Simultaneous study of mechanobiology and calcium dynamics on hESC-derived cardiomyocytes clusters. J. Mol. Recognit. e2760.
Cogollo, J.F.S., Tedesco, M., Martinoia, S., Raiteri, R., 2011. Biomed. Microdevice 13, 613–621.
Dell'Era, P., Benzoni, P., Crescini, E., Valle, M., Xia, E., Consiglio, A., Memo, M., 2015. World J. Stem Cells 7, 329–342.
Doevendans, P.A., Kubalak, S.W., An, R.-H., Becker, D.K., Chien, K.R., Kass, R.S., 2000. J. Mol. Cell. Cardiol. 32, 839–851.
Doppler, S.A., Deutsch, M.A., Lange, R., Krane, M., 2013. J. Thorac. Dis. 5, 683–697.
Fanchaouy, M., Polakova, E., Jung, C., Ogrodnik, J., Shirokova, N., Niggli, E., 2009. Cell Calcium 46, 114–121.
Finsterer, J., Stöllberger, C., 2003. Cardiology 99, 1–19.
Hao, J., Daleo, M.A., Murphy, C.K., Yu, P.B., Ho, J.N., Hu, J., Peterson, R.T., Hatzopoulos, A.K., Hong, C.C., 2008. PLOS One 3, e2904.
Kattman, S.J., Witty, A.D., Gagliardi, M., Dubois, N.C., Niapour, M., Hotta, A., Ellis, J., Keller, G., 2011. Cell Stem Cell 18, 228–240.
Keung, W., Boheler, K.R., Li, R.A., 2014. Stem Cell Res. Ther. 5, 17.
Kilpatrick, J.I., Revenko, I., Rodriguez, B.J., 2015. Adv. Healthc. Mater. 4, 2456–2474.
Knoll, R., Hoshijima, M., Hoffman, H.M., Person, V., Lorenzen-Schmidt, I., Bang, M.L., Hayashi, T., Shiga, N., Yasukawa, H., Schaper, W., McKenna, W., Yokoyama, M., Schork, N.J., Omens, J.H., McCulloch, A.D., Kimura, A., Gregorio, C.C., Poller, W., Schultheiss, P., Chien, K.R., 2002. Cell 111, 943–955.
Laurila, E., Ahola, A., Hyttinen, J., Aalto-Setälä, K., 2015. Biochim Biophys. Acta 1863-7B, 1864–1872.
Lian, X., Zhang, J., Azarin, S.M., Zhu, K., Hazeltine, L.B., Bao, X., Hsiao, C., Kamp, T.J., Palecek, S.P., 2012. Nat. Protoc. 8, 162–175.
Li, Y., Zhang, S., Zhang, X., Li, J., Ai, X., Zhang, L., Yu, D., Yu, D., Ge, S., Peng, Y., Chen, X., 2014. Cardiovasc. Res. 103, 60–71.
Liang, P., Lan, F., Lee, A.S., Gong, T., Sanchez-Freire, V., Wang, Y., Diecke, S., Sallam, K., Knowles, J.W., Wang, P.J., Nguyen, P.K., Bers, D.M., Robbins, R.C., Wu, J.C., 2013. Circulation 127, 1677–1691.
Liu, J., Sun, N., Bruce, M.A., Wu, J.C., Butte, M.J., 2012a. PLoS One 7, e37559.

Liu, Y., Feng, J., Shi, L., Niu, R., Sun, Q., Liu, H., Li, J., Guo, J., Zhu, J., Han, D., 2012b. Nanoscale 4, 99–102.
Ma, J., Guo, L., Fiene, S.J., Anson, B.D., Thomson, J.A., Kamp, T.J., Kolaja, K.L., Swanson, B.J., January, C.T., 2011. Am. J. Physiol. Hear. Circ. Physiol 301, H2006–H2017. https://doi.org/10.1152/ajpheart.00694.2011.
Moretti, A., Laugwitz, K.L., Dorn, T., Sinnecker, D., Mummery, C., 2013. Cold Spring Harb. Perspect. Med. 3.
Motta, B.M., Pramstaller, P.P., Hicks, A.A., Rossini, A., 2017. Stem Cells Int. 2017, 8960236.
Mummery, C.L., Zhang, J., Ng, E.S., Elliott, D.A., Elefanty, A.G., Kamp, T.J., 2012. Circ. Res. 111, 344–358.
Nascimento Osorio, A., Medina Cantillo, J., Camacho Salas, A., Madruga Garrido, M., Vilchez Padill, J.J., 2018. Neurologia. https://doi.org/10.1016/j.nrleng.2018.01.001. (In press).
Pesl, M., Acimovic, I., Pribyl, J., Hezova, R., Vilotic, A., Fauconnier, J., Vrbsky, J., Kruzliak, P., Skladal, P., Kara, T., Rotrekl, V., Lacampagne, A., Dvorak, P., Meli, A.C., Fauconnier, J., Vrbsky, J., Kruzliak, P., Skladal, P., Kara, T., Rotrekl, V., Lacampagne, A., Dvorak, P., Meli, A.C., 2013. Heart Vessels 29, 834–846.
Pesl, M., Ivana, A., Pribyl, J., Hezova, R., Vilotic, A., Aimond, F., Fauconnier, J., Vrbsky, J., Kruzliak, P., Skladal, P., Kara, T., Rotrekl, V., Lacampagne, A., Dvorak, P., Meli, A.C., 2014. Biophys. J. 106 (565A–565A).
Pesl, M., Pribyl, J., Acimovic, I., Vilotic, A.A., Jelinkova, S., Salykin, A., Lacampagne, A., Dvorak, P., Meli, A.C., Skladal, P., Rotrekl, V., 2016a. Biosens. Bioelectron. 85, 751–757.
Pesl, M., Pribyl, J., Caluori, G., Cmiel, V., Acimovic, I., Jelinkova, S., Dvorak, P., Starek, Z., Skladal, P., Rotrekl, V., 2016b. J. Mol. Recognit. 30, e2602.
Regmi, S., Jeong, J.H., 2016. Macromol. Res. 24, 1037–1046.
Rothermel, A., Kurz, R., Ruffer, M., Weigel, W., Jahnke, H.G., Sedello, A.K., Stepan, H., Faber, R., Schulze-Forster, K., Robitzki, A.A., 2005. Cell. Physiol. Biochem. 16, 51–58.
Sinnecker, D., Laugwitz, K.-L.L., Moretti, A., 2014. Pharmacol. Ther. 143, 246–252.
Spira, M.E., Hai, A., 2013. Nat. Nanotechnol. 8, 83–94.
Takeda, M., Miyagawa, S., Fukushima, S., Saito, A., Ito, E., Harada, A., Sawa, Y., 2018. Tissue Eng. C Meth. 24, 56–67.
Tzatzalos, E., Abilez, O.J., Shukla, P., Wu, J.C., 2016. Adv. Drug Deliv. Rev. 96, 234–244.
Vatta, M., Sinagra, G., Brunelli, L., Faulkner, G., 2005. J. Cardiovasc. Med. 10, 149–156.
Wang, T., Hu, N., Cao, J., Wu, J., Su, K., Wang, P., 2013. Biosens. Bioelectron. 49, 9–13.
Youm, J.B., 2016. Integr. Med. Res. 5, 3–10.
Zhang, Y., Sekar, R.B., McCulloch, A.D., Tung, L., 2008. Prog. Biophys. Mol. Biol. 97, 367–382.
Zheng, W., Thorne, N., McKew, J.C., 2013. Drug Discov. Today 18, 1067–1073.